Wide-Band Network Modeling of Interacting Inductive Irises and Steps

T. E. ROZZI AND WOLFGANG F. G. MECKLENBRÄUKER

Abstract—**Methods of field and network theory are jointly applied to the problem of deriving wide-band models for interacting inductive irises and steps in standard and oversize lossless rectangular guides.**

The resulting equivalent network is a cascade of lumped multiports, described by means of their reactance matrix, given in the canonical Foster's form, and of several parallel transmission lines, connecting the interacting discontinuities. The required frequency band and the accuracy of the model can be prescribed at will. The features of the approach are: the solution of the field problem yields a reactance matrix with monotonic convergence properties; small matrices only need be manipulated; the frequency dependence is explicit, so that the field analysis need not be repeated at each frequency point; a true network model (and not a "spot frequency" equivalent circuit) is produced, which is prerequisite for exact synthesis.

I. INTRODUCTION

MANY standard computer oriented methods for solving discontinuity problems in waveguide are based on straightforward modal analysis in terms of two finite sets of normal modes, to be matched on a certain region, and inversion of the resulting matrix equation [1]

A characteristic of this approach is the lack of proper convergence with the increasing order of the double modal expansion. Moreover, the method becomes increasingly unsatisfactory with the number of strongly interacting discontinuities. Quite apart from this, no proper finite equivalent network of the discontinuity is produced.

The importance of a proper wide-band equivalent network is threefold. In the first place, such a model makes repeating the field analysis at each frequency point unnecessary. Secondly, a cascade of interacting discontinuities can be broken down into "building blocks" connected by transmission lines and the field problem of the whole structure can be translated into a network problem. Thirdly, wide-band equivalent networks are prerequisite for the exact synthesis of components and subsystems satisfying given specifications over a given frequency band.

More analytically based methods, such as the variational method [2] and the modified residue technique [3] do not suffer from the convergence difficulties just mentioned. Also, simple variational and quasi-static solutions yield equivalent circuits for *isolated* discontinuities in standard guides which are often fairly accurate in a moderate frequency band [4]. To date, these results are in fact the only ones available to the microwave engineer. However, the stringent requirements of modern telecommunication systems make the characterization of discontinuities by means of accurate wide-band equivalent circuits very desirable.

The principles of a variational approach, which applies methods of both network and field theory to the problem of lossless reciprocal discontinuities in a homogeneous uniform waveguide, were laid down in previous contributions [5]–[7].

In the present paper the approach just mentioned will be pursued and applied to the actual derivation of wide-band equivalent networks of interacting inductive irises and steps in lossless rectangular guides. The guide is standard or moderately oversize. The accuracy of the model as well as the frequency band can be prescribed at will.

Starting from a Rayleigh–Ritz stationary expression for the reactance matrix of the discontinuity, the network representation is derived as a finite lumped multiport with frequency independent elements. In the reactance matrix of the multiport, expressed in the canonical Foster's form, the frequency dependence is explicit, whereas poles and residues depend upon the geometry only. The latter dependence is given in numerical or graphical form or by means of simple interpolatory functions.

The derivation of the model is based upon the following physical considerations. In principle, a discontinuity excites an infinite number of modes. However, if the waveguide is standard or moderately oversize, only a limited number of modes (above or below cutoff) cause appreciable interaction with adjacent discontinuities. These are the "accessible modes" of the discontinuity and correspond to the "accessible ports" of the equivalent network. The number of accessible modes depends, of course, upon the accuracy required of the model. All remaining modes, infinite in number, do not "see" the rest of the circuit; they remain confined to the neighborhood of the discontinuity, there causing energy storage and coupling among the accessible modes. Being well below cutoff, localized modes are almost "lumped" in nature, whereas accessible modes are truly "distributed." It is only natural that accessible and localized modes should be treated in different ways, so as to suit their different properties.

The lossless reciprocal energy storage mechanism of the localized modes is analogous to that of a cavity in all respects [6].

The reactance matrix of an ideal lossless cavity at its accessible ports must satisfy Foster's theorem. Its canonical form is an infinite converging sum of resonant terms.

Manuscript received March 20, 1974; revised July 9, 1974.
The authors are with Philips Research Laboratories, Eindhoven, The Netherlands.

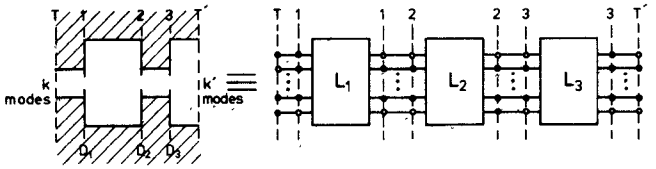

Fig. 1. Cascade of interacting irises (top view) and equivalent network model.

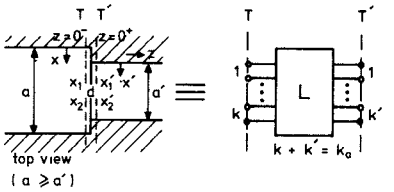

Fig. 2. Geometry of basic discontinuity and its equivalent network.

The unknown poles and residues can, in fact, be extracted from the waveguide admittance, making use of the quasi-static character of the localized modes. This allows the quasi-static limit of the waveguide admittance to be summed exactly for a number of basic configurations, whereas the dynamic correction is a simple function of frequency with constant coefficients. It will be seen that the Rayleigh–Ritz stationary expression of order N for the reactance leads to a Foster's expansion of degree $2N$ Due to its stationary nature, the latter converges rapidly and monotonically with increasing N. Poles and residues are related to the eigenvalues and eigenvectors of the matrix obtained from the waveguide admittance by means of an appropriate expanding set of functions. In practice, manipulations with matrices of small dimension only (typically three or four) are needed.

At this point, the problem of a cascade of interacting discontinuities is translated into the simpler network problem of a cascade of finite multiports connected by lengths of parallel transmission lines (see Fig. 1).

The method just described will be illustrated by means of a few numerical and experimental examples, namely, the infinitely thin interacting iris, the thick iris, the cascade of thick interacting irises, and interacting steps in rectangular waveguides.

II. THE SOLUTION OF THE FIELD PROBLEM

The left-hand side of Fig. 2 illustrates the case of an infinitely thin (a)symmetric iris at a junction of two different waveguides. The practically interesting cases of the infinitely thin iris in a waveguide, the inductive step, and the thick inductive iris are specializations or combinations of the preceding configuration. These will be treated at a later stage.

Let us consider k accessible modes on the left-hand side of the discontinuity and k' on the right-hand side. $k_a = k + k'$ is the total number of accessible modes of the discontinuity. The right-hand side of Fig. 2 shows the equivalent lumped network representation of the discontinuity as a k_a port. The reference planes of the accessible modes are placed *at the location of the discontinuity*. The finite lumped multiport L represents the energy storage of the localized modes in the neighborhood of the discontinuity. Since the guide is uniform and lossless, coupling between accessible modes takes place only at the location of the discontinuity and is described via the multiport L.

With reference to Fig. 2, let us define:

$\Gamma_n = [(n\pi/a)^2 - (2\pi/\lambda)^2]^{1/2}$, $(\Gamma_1 = j\beta)$ — propagation constant of the TE_{no} mode on the left-hand guide

$\Gamma_m' = [(m\pi/a')^2 - (2\pi/\lambda)^2]^{1/2}$ — propagation constant of the TE_{mo} mode on the right-hand guide.

The characteristic admittance of the TE_{no} mode, normalized to the free space admittance, is $\Gamma_n/j\omega\mu_0$ so that the characteristic admittance of the TE_{10} mode (in the larger guide) is $\beta/\omega\mu_0$. The energy stored in the localized modes can be computed from the susceptive part of the modified magnetic Green's function at $z = z' = 0$. This can be written as the sum of the contribution due to the left half-guide and that of the right half-guide [5]. These expressions can be found in a standard textbook, such as Collin's [8]. In our case, however, the localized modes only contribute to the sum, since the accessible modes are treated separately by means of transmission lines.

In order to obtain good convergence properties, we transform the original kernel as described in [8,p.349] (see also Appendix I). The susceptive part, normalized to the characteristic admittance of the TE_{10} mode in the larger guide, within a factor $(a/\pi)^2$ which disappears at a later stage, is

$$\boldsymbol{B}(x,\xi) = \sum_{n>k} \frac{1}{n^2}\frac{\Gamma_n}{\beta}\varphi_n(x)\varphi_n(\xi) + \frac{a'}{a}\sum_{m>k'}\frac{1}{m^2}\frac{\Gamma_m'}{\beta}\psi_m(x)\psi_m(\xi). \quad (1)$$

φ_n and ψ_m are related to the eigenfunctions of the two guides:

$$\varphi_n(x) = \cos\frac{n\pi}{a}x$$

$$\psi_m(x) = \cos\frac{m\pi x'}{a'} = \cos\frac{m\pi}{a'}(x + x_1' - x_1).$$

It is convenient to separate in (1) the quasi-static limit ($(a/\lambda)^2 \to 0$) and the "dynamic correction:"

$$\boldsymbol{B}(x,\xi) = \boldsymbol{B}^s + \boldsymbol{B}^d = \sum_{n>k}\frac{1}{\beta}\frac{1}{n^2}\frac{n\pi}{a}\varphi_n(x)\varphi_n(\xi) + \frac{a'}{a}\sum_{m>k'}\frac{1}{\beta}\frac{1}{m^2}\frac{m\pi}{a'}\psi_m(x)\psi_m(\xi) + \sum_{n>k}\frac{1}{\beta}\frac{\Gamma_n - n\pi/a}{n^2}\varphi_n(x)\varphi_n(\xi) + \frac{a'}{a}\sum_{m>k'}\frac{1}{\beta}\frac{\Gamma_m' - m\pi/a'}{m^2}\psi_m(x)\psi_m(\xi). \quad (2)$$

Further, we introduce the transformation due to Schwinger [3], [8], [9]

$$\cos\frac{\pi x}{a} = P_{10} + P_{11}\cos\vartheta := \alpha_1 + \alpha_2\cos\vartheta$$

with

$$P_{10} := \alpha_1 := \cos\frac{\pi d}{2a}\cdot\cos\pi\frac{2x_1 + d}{2a}$$

$$P_{11} := \alpha_2 := \sin\frac{\pi d}{2a}\cdot\sin\pi\frac{2x_1 + d}{2a} \quad .$$

With the preceding transformation, we have

$$\cos\frac{n\pi}{a}x = \sum_{p=0}^{n} P_{np}\cos p\vartheta. \tag{3}$$

The coefficients of the *finite* summation (3) are given in Appendix II.

With the same expanding set, we also obtain

$$\cos\frac{m\pi}{a'}x' = \sum_{p=0}^{\infty} A_{mp}\cos p\vartheta \tag{4}$$

where

$$A_{mp} = \frac{(2-\delta_{op})}{\pi}\int_0^{\pi}\cos\frac{m\pi}{a'}x'(\vartheta)\cdot\cos p\vartheta\cdot d\vartheta. \tag{5}$$

Substituting (3) and (4) into (2) and proceeding analogously to [8,p.341–343], we obtain a new expression for the aperture in terms of the new variables ϑ,η:

$$\boldsymbol{B}(\vartheta,\eta) = \sum_{p,q=0}^{\infty} B_{pq}\cos p\vartheta\cdot\cos q\eta$$

where

$$B_{pq} = B_{pq}{}^{s} + B_{pq}{}^{d} \tag{6}$$

and

$$B_{pq}{}^{s} = \frac{\pi}{a\beta}\left[\epsilon_{pq} - \sum_{n=1}^{k}\frac{1}{n}P_{np}P_{nq}\right] + \frac{\pi}{a\beta}\left[\sum_{m>k'}\frac{1}{m}A_{mp}A_{mq}\right] \tag{7}$$

with

$$\epsilon_{pq} = \begin{cases} 0, & \text{for } p \neq q \\ -2\ln\alpha_2, & \text{for } p = q = 0 \\ 1/p, & \text{for } p = q > 0 \end{cases}$$

$$B_{pq}{}^{d} = \frac{1}{\beta}\left[\sum_{n>k}\frac{1}{n^2}\left(\Gamma_n - \frac{n\pi}{a}\right)P_{np}P_{nq}\right] + \frac{1}{\beta}\frac{a'}{a}\left[\sum_{m>k'}\frac{1}{m^2}\left(\Gamma_{m'} - \frac{m\pi}{a'}\right)A_{mp}A_{mq}\right]. \tag{8}$$

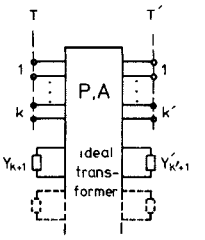

Fig. 3. Infinite transformer network coupling the waveguide modes.

It can be seen from (7) that the quasi-static contribution of the larger guide, which is in fact also the largest one, is given as a finite sum by means of the preceding transformation. The remaining three summations must be carried out numerically.

The infinite dimensional matrix B, defined in (6), corresponds to $\boldsymbol{B}$ in the "basis" introduced by Schwinger's transformation. The latter induces an infinite equivalent network of the fields *on* the aperture. B is the susceptance matrix, corresponding to the energy storage in the guides as seen on the aperture.

Fig. 3 illustrates the network interpretation. The "basis" on the aperture can be seen as an ideal transformer with an infinite number of ports. All ports corresponding to localized modes have been terminated by their modal characteristic admittances. Energy storage takes place only in these reactive terminations, while coupling between all modes, in particular between the accessible modes, takes place via the transformer, where no energy is stored. The matrices P and A are just the transformer ratio matrices.

Although infinite in principle ($0 \leq p,q \cdots \infty$), B must be truncated to a finite order N in order to compute its inverse, which appears in the following equations. This is equivalent to assuming a finite field expansion on the aperture and therefore *rectangular* ($N \times \infty$) transformer ratio matrices appear.

Finite truncation of the matrix B is independent of the computation of the original kernel (the stored energy). This is at the origin of the good convergence properties of the expression for the (normalized) reactance matrix of the k_a port L, describing how the discontinuity is seen by the accessible modes [6].

$$X_{ij} = \tau_i\tau_j Q^{T}{}_{*i}\cdot B^{-1}\cdot Q_{*j} \tag{9}$$

Q_{*i} denotes the ith column of the matrix P^T if $i \leq k$ or the $(i\text{-}k)$th column of A^T if $i > k$. Also,

$$\tau_i = \begin{cases} \dfrac{1}{i}, & \text{for } 1 \leq i \leq k \\ \dfrac{1}{(i-k)}\,(a'/a)^{1/2}, & \text{for } k+1 \leq i \leq k_a. \end{cases}$$

The factor $\tau_i\tau_j$ is introduced as a consequence of the transformation used prior to obtaining (1) (see Appendix I). Expression (9) is in fact identical with the Rayleigh–Ritz variational solution of order N [6],

III. FREQUENCY DEPENDENCE AND FOSTER'S FORM

Localized modes are characterized by the fact that their propagation constants are real large numbers ($\Gamma_n \rightarrow n\pi/a$, as $n \rightarrow \infty$). Physically, this implies that the fields pertaining to these modes remain in the neighborhood of the discontinuity, where their excitation takes place, so that these modes cause no interaction between neighboring discontinuities. In intuitive terms, they do not "see" the neighboring discontinuities. Therefore, one could imagine that magnetic walls, for these modes only, are placed long, but finite, distances away from the discontinuity. One visualizes the space enclosed between these magnetic walls and the waveguide walls as forming an ideal cavity, storing the energy of the localized modes. The magnetic wall boundary conditions are consistent with a reactance matrix description. Coupling of the cavity to the external world takes place on the aperture of the discontinuity, via the accessible modes.

As a function of frequency, the reactance matrix of a lossless reciprocal cavity with k_a accessible ports must have the form

$$X_{ij}(\omega) = \sum_{m=1}^{\infty} \frac{\omega r_{ij}^{(m)}}{1 - (\omega/\omega_m)^2}, \qquad 1 \leq i,j \leq k_a \tag{10}$$

with $\omega_m \simeq 0(m)$ and $r_{ij}^{(m)} \rightarrow 0$ as $m \rightarrow \infty$. Also, the constant residue matrices $r^{(m)}$ are nonnegative definite [10], [11]. Normalization to the characteristic impedance of the larger guide merely replaces X by $\bar{X}$, i.e.,

$$\bar{X}(\omega) = \beta/\omega\mu_0 X(\omega).$$

One should observe that, within a normalization constant, (9) and (10) are two independent expressions for the same reactance matrix. In particular, in expression (9), obtained from a waveguide description, the dependence on the geometry and on frequency are connected in a very complicated way. On the other hand in (10), the frequency dependence is given explicitly, while poles and residues are functions of the geometry only. These functions are unknown as yet. However, they can be extracted from (9). In the following, we shall derive from (9) a finite approximation to (10). This is based on the "quasi-static" behavior of the localized modes and the fact that in (8) the frequency dependence is only contained in the factors Γ_n, Γ_m', and β.

Let us now investigate the frequency dependence of the function $\Gamma_n(\omega)/\beta(\omega)$ $(n > k \geq 1)$. We have

$$\frac{\Gamma_n(\omega)}{\beta(\omega)} = \frac{n\pi/a}{\pi/a} \frac{[1 - (1/n^2)(2a/\lambda)^2]^{1/2}}{[(2a/\lambda)^2 - 1]^{1/2}}$$

$$= n\frac{[1 - (\bar{\omega}/n)^2]^{1/2}}{(\bar{\omega}^2 - 1)^{1/2}}. \tag{11}$$

Here we have introduced the normalized frequency $\bar{\omega} = \lambda_c/\lambda = 2a/\lambda$, $\lambda_c = 2a$ being the cutoff wavelength of the ground mode in the larger guide. With this normalization, the ordinary guide bandwidth is given by $1 \leq \bar{\omega} \leq 2$. To the first two terms, the series expansion of the square root of the numerator of (11) is

$$\left(1 - \frac{\bar{\omega}^2}{n^2}\right)^{1/2} \simeq 1 - \frac{1}{2}\frac{\bar{\omega}^2}{n^2}. \tag{12}$$

This is a good approximation for $(\bar{\omega}/n)^2 \ll 1$, as it is the case for all localized modes except, possibly, the first few. Furthermore, the functional form of the preceding approximation has the advantage of being very convenient for deriving the Foster's form of the reactance, as will be seen later. In particular, going over to the complex frequency $p = \sigma + j\omega$ it is evident that the expression

$$\frac{\Gamma_n(p)}{\mu_0 p} \simeq \frac{n\pi}{\mu_0 a}\left(\frac{1}{p} + \frac{1}{2}\frac{p}{n^2}\right)$$

is a positive real approximation to the input admittance of a lossless one-port network (the characteristic admittance of the nth mode). If only the ground mode is considered accessible, (12) may not be always sufficient to provide a satisfactory approximation in the frequency band of interest.

With a view to improving the approximation while still maintaining the convenient functional form of the right-hand side of (12), let us slightly modify the latter as follows:

$$\left(1 - \frac{\bar{\omega}^2}{n^2}\right)^{1/2} \simeq k_1^{(n)} - \frac{k_2^{(n)}}{2}\frac{\bar{\omega}^2}{n^2} \tag{13}$$

with positive constant $k_1^{(n)}$, $k_2^{(n)}$ $(\rightarrow 1$ as $n \rightarrow \infty)$. For given n, the free parameters k_1,k_2 can be determined from the associated problem of approximating Γ_n/β by $(n\pi/a)$ $[k_1^{(n)} - (k_2^{(n)}/2)(\bar{\omega}^2/n^2)]/\beta$ in the Chebyshev sense over the frequency band of interest. To give an impression of the accuracy accruing by means of the preceding approach, consider a typical example: $n = 3$, $1.2 \leq \bar{\omega} \leq 2$. Using the original expression (12), the maximum relative error in the band is 1.5 percent, whereas, using (13) with $k_1 = 1.014$, $k_2 = 1.194$ yields a maximum relative error equal to 1.3 per mil. The accuracy of the approximation improves rapidly either by increasing n or reducing the frequency band.

A similar approximation gives *a fortiori* better results when applied to the propagation constant in the smaller guide:

$$\Gamma_{m'} = \frac{m\pi}{a'}\left[1 - \left(\frac{a'}{a}\frac{\bar{\omega}}{m}\right)^2\right]^{1/2}, \qquad (a' \leq a).$$

Introducing (13) in (8), we obtain from (7) and (8) the following susceptance matrix:

$$B = \frac{1}{\beta}[C^s - \bar{\omega}^2 C^d] \tag{14}$$

where

$$C_{pq}{}^{s} = \frac{\pi}{a}\left[\epsilon_{pq} - \sum_{n=1}^{k}\frac{1}{n}P_{np}P_{nq} + \sum_{n>k}\frac{k_1{}^{(n)} - 1}{n}P_{np}P_{nq}\right] + \frac{\pi}{a}\left[\sum_{m>k'}\frac{k_1{}'^{(m)}}{m}A_{mp}A_{mq}\right] \quad (15)$$

$$C_{pq}{}^{d} = \frac{1}{2}\frac{\pi}{a}\left[\sum_{n>1}\frac{k_2{}^{(n)}}{n}P_{np}P_{nq} + \left(\frac{a'}{a}\right)^{2}\sum_{m>k'}\frac{k_2{}'^{(m)}}{m^3}A_{mp}A_{mq}\right]. \quad (16)$$

Since B is the susceptance matrix of a lossless reciprocal structure, the matrices C^s and C^d are symmetric and nonnegative definite. Furthermore, the matrix C^s being the dc-residue matrix of B is positive definite.

This implies in turn that the two matrices can be diagonalized simultaneously. In order to do so, let us rewrite βB in (14) as

$$\begin{aligned}\beta B &= (C^s)^{1/2}[1 - \bar{\omega}^2\,(C^s)^{-1/2}C^d(C^s)^{-1/2}](C^s)^{1/2}\\ &= (C^s)^{1/2}[1 - \bar{\omega}^2 T\Lambda T^T](C^s)^{1/2}\\ &= (C^s)^{1/2}T(1 - \bar{\omega}^2\Lambda)\,T^T(C^s)^{1/2}\\ &= M^{-1}(1 - \bar{\omega}^2\Lambda)\,(M^{-1})^T \end{aligned} \quad (17)$$

where the matrix $(C^s)^{1/2}$ is the symmetric "square root" of C^s, T is the orthogonal matrix of the eigenvectors of $(C^s)^{-1/2}C^d(C^s)^{-1/2}$, and Λ is the diagonal matrix of the corresponding positive eigenvalues. Introducing now (17) in (9) we obtain the (normalized) reactance matrix of the discontinuity as

$$\begin{aligned}\bar{X}_{ij}(\bar{\omega}) &= \tau_i\tau_j Q_{*i}{}^{T}\cdot B^{-1}\cdot Q_{*j}\\ &= \tau_i\tau_j\beta Q_{*i}{}^{T}\cdot M^{T}\cdot(1 - \bar{\omega}^2\Lambda)^{-1}\cdot M\cdot Q_{*j}\\ &= \tau_i\tau_j\beta\sum_{m=1}^{N}\frac{(MQ_{*i})_m\cdot(MQ_{*j})_m}{1 - (\bar{\omega}/\bar{\omega}_m)^2}\\ &= \beta\sum_{m=1}^{N}\frac{r_{ij}{}^{(m)}}{1 - (\bar{\omega}/\bar{\omega}_m)^2}\end{aligned} \quad (18)$$

where $\Lambda = \mathrm{diag}\ (1/\bar{\omega}_m{}^2)$. Equation (18) is the required finite approximation to the Foster's form (10).

As mentioned already in connection with (10), the cavity model implies: $\bar{\omega}_1{}^2 < \bar{\omega}_2{}^2 < \cdots < \bar{\omega}_N{}^2 = 0(N^2)$. Furthermore, the first resonant frequency is much higher than the upper limit of the frequency band of operation. This is a consequence of the choice of the reference planes and of the quasi-static behavior of the localized modes.

In (18), the frequency dependence of the reactance matrix has been separated from the geometry dependence. The latter is contained in the poles and the residues. Repeating the field analysis at each frequency point is therefore no longer necessary. Field analysis has provided us with a true finite network model valid over a prescribed frequency band (in contrast with a "spot-frequency" Weissfloch's equivalent circuit [8, p.251]). The study of the frequency characteristics of the isolated discontinuity and its interaction with other discontinuities follows now on the basis of standard network analysis.

In the following, we shall apply the preceding theory to the problem of building an accurate network model of waveguide components such as filters, transformers, and cascades of inductive steps in general. We will begin with the basic "building blocks" such as the infinitely thin symmetric inductive iris, the waveguide H-plane step, and the thick inductive iris.

IV. THE INFINITELY THIN SYMMETRIC INDUCTIVE IRIS IN WAVEGUIDE

A top view of the configuration is shown in Fig. 4(a), while Fig. 4(b) gives a four-port model of the discontinuity. This model is applicable to the case where the TE_{10} mode of the guide is above cutoff, whereas the first nonpropagating mode, the TE_{30} mode, may still cause appreciable interaction with neighboring discontinuities.

This choice will prove sufficient in most cases, since in most practical situations, interaction via the first nonpropagating mode only is of any importance. The typical range of application corresponds to an iris to iris distance $\approx a/2$ for the worst case of higher order mode excitation $(d/a = 0.5)$. In fact, a two-port description is often sufficient. This case can be easily recovered from the more general one presented here by closing the two TE_{30} ports by the corresponding characteristic admittances.

The TE_{10} and TE_{30} modes are the "accessible modes" in the sense discussed in the previous section. The remaining TE_{no} modes (with n odd, >3) are the localized modes.

Since the semi-infinite guide on the left is identical to that on the right, expressions (15) and (16) for the matrices C^s and C^d in (14), now reduce to

$$C_{pq}{}^{s} = \frac{2\pi}{a}\left[\epsilon_{pq} - \sum_{n=1,3}\frac{1}{n}P_{np}P_{nq} + \sum_{n>3;\,n\ \mathrm{odd}}\frac{k_1{}^{(n)} - 1}{n}P_{np}P_{nq}\right] \quad (19)$$

and

$$C_{pq}{}^{d} = \frac{\pi}{a}\left[\sum_{n>3;\,n\ \mathrm{odd}}\frac{k_2{}^{(n)}}{n^3}P_{np}P_{nq}\right]. \quad (20)$$

One sees from (2) and Appendix I that in this case, as a consequence of the iris being symmetric, $P_{np} = 0$ whenever p is even. At this point, it is convenient to renumber the indices, so that $p = 2p' - 1$, $q = 2q' - 1$; $p',q' = 1,2,\cdots N$. N is the dimension of the finite truncation of the matrix B, which is also the order of the finite approximation of the reactance matrix X in (10).

Symmetry about the plane $z = 0$ and reciprocity of the structure imply that X must have the form

$$\begin{pmatrix} x_1 & x_2 \\ x_2{}^{T} & x_1 \end{pmatrix} \quad (21)$$

where x_1,x_2 are 2×2 submatrices and x_1 is symmetric. The fact that the obstacle is infinitely thin further implies that

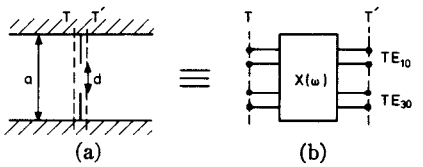

Fig. 4. Infinitely thin iris (top view) and the model considered.

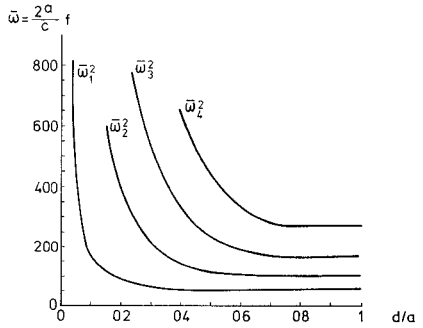

Fig. 5. Poles of the fourth order representation of the thin iris.

$x_1 = x_2 = x'$. This could also be seen by direct inspection of (18), specialized to the case of interest. Our problem is thus reduced to finding the poles and residues of the symmetric 2×2 matrix $x'(\bar{\omega})$. In the subsequent numerical example N was fixed equal to four. This choice was motivated by the fact that taking a higher value of N did not affect the results significantly. Following the steps indicated in (17) and (18), the four poles and the corresponding residue matrices were computed as functions of the only geometrical parameter d/a. Poles are plotted in Fig. 5 The corresponding residues are plotted in Fig 6(a)–(c).

With the help of these graphs, the reactance matrix of any thin inductive iris can be constructed without having recourse to a computer program. The functions $\bar{\omega}_m(d/a)$ and $r_{ij}^{(m)}(d/a)$ can very well be approximated by the empirical formulas

$$\bar{\omega}_m^2(d/a) \simeq a_m \coth\left(b_m \tan\frac{\pi}{2}\frac{d}{a}\right) \tag{22a}$$

$$r_{ij}^{(m)}(d/a) \simeq c_{ij}^{(m)} \sinh\left(d_{ij}^{(m)}\frac{d}{a}\right) \tag{22b}$$

with constants a_m, b_m, $c^{(m)}$, $d^{(m)}$ to be determined by fitting in the range of interest.

V. THE SYMMETRIC H-PLANE STEP AND THE THICK INDUCTIVE IRIS

The top view of a symmetric H-plane step is illustrated in Fig. 2, if $a' = d$ and $x_2 = a - x_1$. Introducing $a' = d$ in (5) and (7), these formulas apply as they stand. Again, the discontinuity depends upon one geometrical parameter only: d/a. We can build a four-port equivalent network of the discontinuity for the TE_{10} and TE_{30} modes at each side of the junction, where poles and residues of the reactance matrix of the four-port are functions of d/a. The analysis follows closely the same lines as for the thin iris, except that the four-port is no longer symmetric.

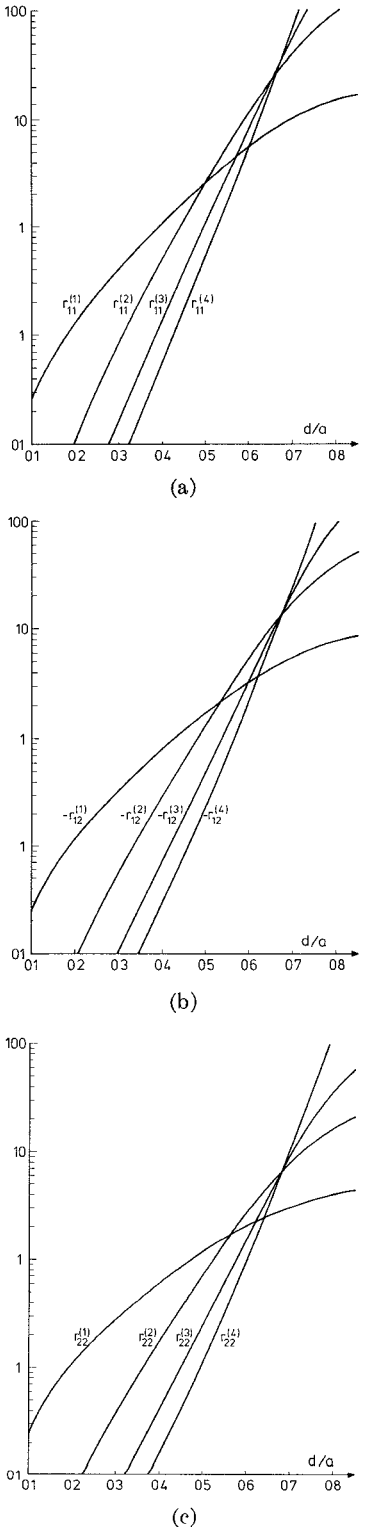

Fig. 6. Corresponding residues.

The thick inductive iris can be considered as being constituted by two opposite steps separated by a length $2t$ of iris "waveguide," as shown in Fig. 7. The number k' of accessible modes in the iris must be chosen according to the ratios d/a and t/a. The thickness effect is taken into account of by means of the k' transmission lines in the iris (accessible modes between two steps). All higher order

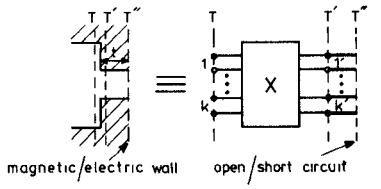

(a) (b)

Fig. 7. The thick iris as a double step discontinuity.

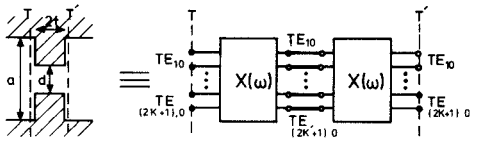

(a) (b)

Fig. 8. Even/odd mode problems for the thick iris.

iris modes excited by the steps are terminated by their characteristic admittances, i.e., they do not "see" the other step.

We can build an alternative model for the thick iris in a waveguide since this structure is symmetric with respect to $z = 0$ and can be analyzed in terms of the even and odd excitation modes. The even and odd mode half-structures are obtained by placing a magnetic or an electric wall at the plane of longitudinal symmetry falling in the middle of the iris, as shown in Fig. 8. This is in fact a step problem where the modes on the right are terminated by an open/short circuit after a distance t of transmission line.

Accordingly, the admittance matrix B for the even/odd mode is given by the formulas (7) and (8) where for all localized modes in the iris Γ_m'/β is now replaced by

$$\Gamma_m'/\beta \begin{cases} \tanh \Gamma_m' t \\ \coth \Gamma_m' t \end{cases}$$

for the even/odd mode, respectively.

Again, owing to the weak frequency dependence of the localized modes, we can approximate

$$\Gamma_m' \begin{cases} \tanh \Gamma_m' t \\ \coth \Gamma_m' t \end{cases}$$

by an expression like (13), where $k_{1e,o}'^{(m)}$, $k_{2e,o}'^{(m)}$ ($\to 1$ as $m \to \infty$) are determined by a Chebyshev approximation in the band of interest, for the even and odd mode separately. The resulting expressions for the matrices C^s and C^d are

$$C_{pq}{}^s = \frac{\pi}{a}\Bigg[\epsilon_{pq} - \sum_{n=1,3}^{2k-1} \frac{1}{n} P_{np}P_{nq} + \sum_{n>2k-1;n \text{ odd}} \frac{-k_1^{(n)} - 1}{n} P_{np}P_{nq} + \sum_{m>2k'-1;m \text{ odd}} \frac{A_{mp}A_{mq}}{m} \begin{cases} k_{1,e}'^{(m)} \tanh (m\pi/d)t \\ k_{1,0}'^{(m)} \coth (m\pi/d)t \end{cases}\Bigg] \tag{23}$$

$$C_{pq}{}^d = \frac{\pi}{2a}\Bigg[\sum_{n>2k-1;n \text{ odd}} \frac{k_2^{(n)}}{n^3} P_{np}P_{nq} + \left(\frac{d}{a}\right)^2 \sum_{m>2k'-1,m \text{ odd}} \frac{1}{m^3} A_{mp}A_{mq} \cdot \begin{cases} k_{2,e}'^{(m)} \left(\tanh \frac{m\pi}{d} t + \frac{m\pi t/d}{\cosh^2 (m\pi/d)t}\right) \\ k_{2,0}'^{(m)} \left(\coth \frac{m\pi}{d} t - \frac{m\pi t/d}{\sinh^2 (m\pi/d)t}\right) \end{cases}\Bigg]. \tag{24}$$

The upper expression holds for the even case, the lower one for the odd case. Observe that for $\pi t/d \gg 1$ the expressions for the even and odd case in (23) and (24) approach their common value given by (15) and (16), respectively (set $d = a'$). Starting from (23), (24), we can repeat the same steps as in Section III, leading from (14) to (18). We thus obtain the reactance matrices X_e', X_o' of the k_a-port representation, shown in Fig. 8(a), at the reference planes $T - T'$.

If no iris mode is above cutoff, then $k' = 0$ in the above formulas and $k_a = k$. If some iris modes are above cutoff, we can eliminate them from the network representation by closing them with the appropriate terminations. Standard network analysis yields the following formulas for the $k \times k$ driving point reactance matrices X_e, X_o at the reference planes T:

$$X_u = (x_u')_{11} - (x_u')_{12} \cdot \Bigg[(x_u')_{22} + \frac{1}{\beta} \operatorname{diag}\left(\Gamma_1' \begin{cases} \tanh \Gamma_1' t \\ \coth \Gamma_1' t \end{cases}, \cdots, \Gamma'_{2k'-1} \begin{cases} \tanh (\Gamma'_{2k'-1}t) \\ \coth (\Gamma'_{2k'-1}t) \end{cases}\right)^{-1} (x_u')_{12}{}^T \tag{25}$$

where

$$x_u' = \begin{matrix} \\ k \\ k' \end{matrix} \overbrace{\begin{matrix} k & k' \\ \end{matrix}} \begin{pmatrix} (x_u')_{11} & (x_u')_{12} \\ (x_u')_{12}{}^T & (x_u')_{22} \end{pmatrix}.$$

u stands for e in the even case and the upper expressions in (25) should be used, u stands for o in the odd case and the lower expressions should be used.

Finally, the $2k \times 2k$ reactance matrix of the thick iris can be expressed in terms of the even/odd mode $k \times k$ reactance matrices as

$$X = \frac{1}{2}\begin{pmatrix} X_e + X_o & X_e - X_o \\ X_e{}^T - X_o{}^T & X_e + X_o \end{pmatrix}. \tag{26}$$

The approach just described entails repeating the analysis for the even and the odd cases. Furthermore, poles and residues of the reactance matrices X_e, X_o are now (weak)

functions of t/a as well as of d/a, whereas in the case of the step, the only geometrical parameter was d/a. With respect to the double step approach previously discussed, the advantage of the latter approach consists in the fact that fewer accessible ports need be considered in the case of thin irises, which is the one most frequently encountered in the applications. In particular, if the iris is below cutoff, then no mode at all need be considered as accessible in the iris. The port reduction expressed by formula (25) is then no longer necessary.

An example of the latter will be discussed in the following section.

TABLE I

even			
m	1	2	3
ω_m^2	9.27	51.77	233.38
$r_{TE}^{(m)}$	0.630	0.0234	0.00506
odd			
ω_m^2	124.19	244.94	459.05
$r^{(m)}$	0.0108	0.0318	0.0154

frequency band: $1 < \bar{\omega} < 2$ ($\bar{\omega} = 1$: cutoff TE_{10}; $\bar{\omega} = 2$: cutoff TE_{20})

VI. FURTHER NUMERICAL AND EXPERIMENTAL RESULTS

The application of the theory presented in the previous sections will now be demonstrated by means of a few examples.

1) The Isolated Thick Iris in the Standard Waveguide Band ($1 < \bar{\omega} < 2$): Table I gives poles and residues of the even and odd mode reactances for $d/a = 0.5$ and $2t/a = 0.5$. Although fairly typical in practice, these dimensions represent a "worst case" for the existing approximate representations of the iris. In fact, the preceding ratio d/a corresponds to maximum higher order mode excitation and the thickness, while being too large to be neglected, is at the same time too small to be taken care of by means of a single iris mode. In the computation, no accessible modes were assumed in the iris [$k' = 0$ in (23), (24)]. Also, N was set equal to 3 in (18) and only one accessible mode was assumed in the guide ($k = 1$). Table I shows how rapidly the Foster's representation converges. Only the first resonant frequency of the even mode needs be taken into account. The contribution of all other terms can be lumped in static inductances.

The equivalent network of Fig. 9(a), is based upon the approximation just mentioned. It holds in the ranges: $0.1 \leq d/a \leq 0.5$ for $2t/a \leq 0.05$ and $0.2 \leq d/a \leq 0.5$ for $2t/a \leq 0.1$.

In Fig. 9(b)–(e) the element values of Fig. 9(a) are plotted in the preceding range. Outside this range, more than one resonant frequency (or no resonant frequency) need be taken into account. Negative inductances L_3, together with positive inductances L_1, can be interpreted as belonging to a realizable transformer ($L_1 + 2L_3 > 0$). This occurs due to the thickness effect.

2) A Cascade of Thick Interacting Inductive Irises: The field problem of a cascade of interacting irises has been reduced to the network problem of analyzing a cascade of lumped multiports connected by a finite and (small) number of transmission lines, as shown in Fig. 1.

In the range of interest, the multiports are described by their canonical Foster's form, explicitly displaying the frequency dependence. Poles and residues depend upon the geometry only and are obtained by means of field analysis. Propagation constants and characterisitic admittances of the transmission lines, describing the accessible modes, are known. Therefore, we can apply standard network analysis in order to obtain the frequency characteristics of the cascade. In order to check the theory, an accurate experimental structure, consisting of a cascade of eight interacting irises, was built and tested. Numerical and experimental results are shown in Fig. 10. The figure shows VSWR versus frequency in the range 19–21 GHz. The thinner line was computed with the thick iris approach described in the previous section. A fourth order trial field ($N = 4$) was assumed on all apertures. Two modes: TE_{10}, above cutoff, and TE_{30}, below cutoff, but still causing interaction, were considered accessible in the sections of waveguide. One mode: TE_{10}, below cutoff, was assumed accessible in the iris, in the even/odd mode representation of the iris. Taking N equal to 3, 5, or 6 changed the characteristics only slightly. This is a consequence of the stationary nature of the reactance of each iris. The thicker line is the envelope of experimental points obtained by slotted-line measurements. The agreement can be considered excellent for a structure of this complexity. The 3-percent error in bandwidth and the slight peak deformation appearing at the upper band edge can be attributed to tolerance variations in the guide width along the structure, since the guide width was assumed constant in the computation. Also, no account was taken of losses and of residual geometrical imperfections such as asymmetries, misalignment, and bending of the irises.

Interaction between adjacent irises via the TE_{30} mode is a relatively weak effect in the structure just mentioned. The influence of interaction between adjacent discontinuities will be illustrated in the following examples, where the effects appear in increasing measure.

3) H-Plane Oversize Section: Consider Fig. 11. The continuous line represents the computed modulus of the reflection coefficient for the TE_{10} mode versus frequency of an H-plane oversize section in a standard X-band waveguide. The dimensions are given in the figure. The reader is cautioned that, consistent with the previous use, a' denotes the width of the smaller guide. As it happens, a' is now the standard waveguide width. The frequency ranges from 6.5 to 19 GHz. Above this frequency (namely, at 19.7 GHz), the TE_{30} mode in the standard guide becomes propagating and a two-port model for the input–output relation no longer applies.

A sixth order trial field was assumed on the aperture. Two modes were considered accessible in both sections of

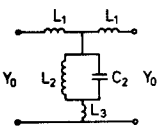

$$L_1 = \sum_{m=1}^{N} r_\sigma^{(m)}$$

$$L_2 = \tfrac{1}{2} r_e^{(1)} \qquad C_2 = \frac{1}{\omega_{1,\infty}^2 L_2}$$

$$L_3 = \tfrac{1}{2}\left(\sum_{m=2}^{N} r_e^{(m)} - \sum_{m=1}^{N} r_\sigma^{(m)}\right)$$

$$\tilde{\omega} = \frac{2a}{\lambda} = \frac{\lambda_c}{\lambda}, \qquad y_0 = \tfrac{1}{\beta}\sqrt{\tilde{\omega}^2 - 1}.$$

$1 \leqslant \tilde{\omega} \leqslant 2$, $2t/a \leqslant 0.05$ for $0.1 \leqslant d/a \leqslant 0.5$,
$2t/a \leqslant 0.1$ for $0.2 \leqslant d/a \leqslant 0.5$,

(a)

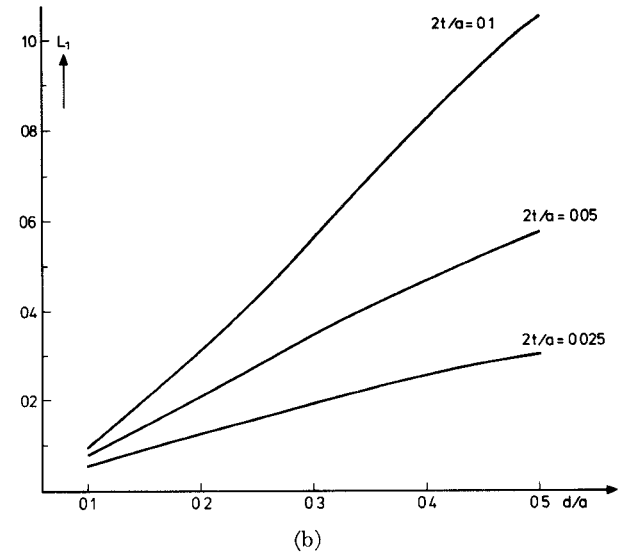

(b)

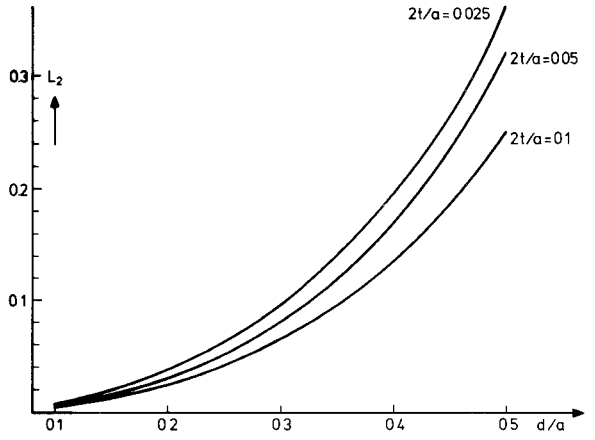

(c)

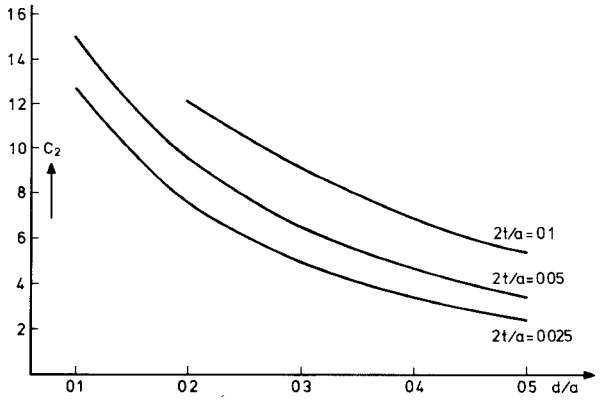

(d)

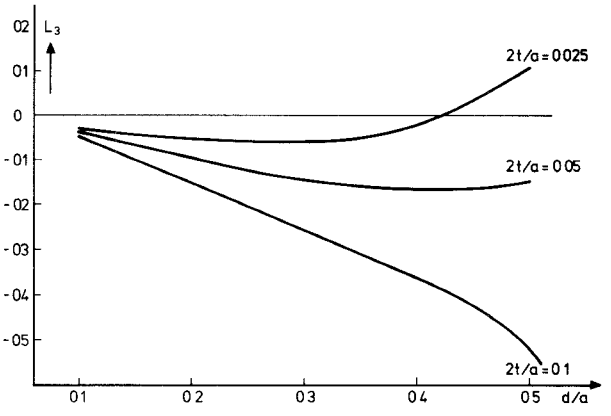

(e)

Fig. 9. Simplified equivalent circuit and element values versus geometry.

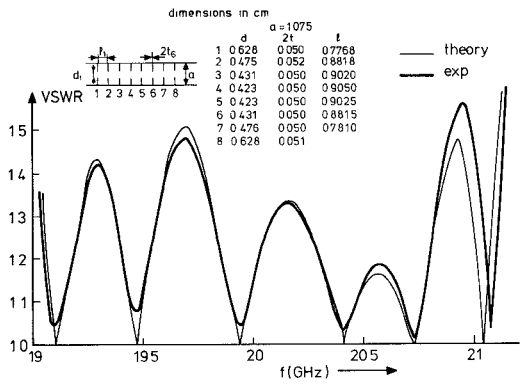

Fig. 10. Cascade of eight thick interacting irises.

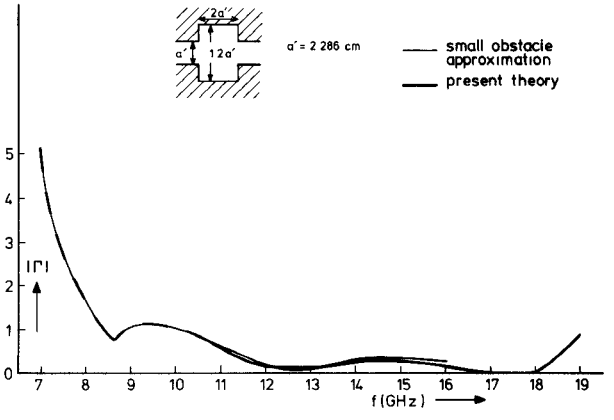

Fig. 11. A "small" double step discontinuity.

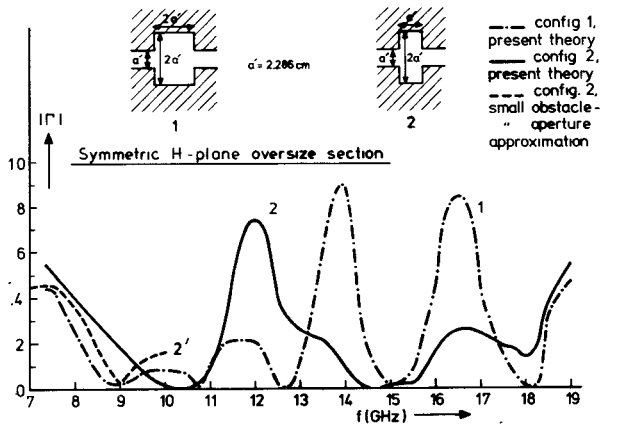

Fig. 12. Large double step discontinuity.

guide. In this example the ratio a'/a is close to unity ($1 - a'/a = 0.166$) and the distance between the discontinuities is relatively large ($t/a = 1$). Therefore, Marcuvitz's small obstacle formulas [4] are expected to be quite accurate up to almost the cutoff frequency of the TE_{30} mode in the larger section (16.3 GHz). The thinner curve in Fig. 11 indeed gives the result computed according to [4]. It is seen that the two curves are virtually identical in the lower part of the band. Even at higher frequencies, the agreement is very close. However, whereas Marcuvitz's approach is necessarily limited to the bandwidth, $1 < 2a'/\lambda < 2a/\lambda < 3$, no such restriction is posed in principle on the method presented.

Fig. 12 contrasts the behavior of two identical large double steps placed at two different distances. Curve 1 refers to the left-hand side insert in the figure. Here $a'/a = 0.5$ and the distance is identical to that used in the previous example. At 10 GHz two modes become propagating in the larger guide. The two peaks occurring at 14 and 16 GHz, respectively, are due to destructive interference between the TE_{10} and the TE_{30} modes. The possible occurrence of this effect was in fact qualitatively predicted by Butterweck [12].

Curve 2 refers to a similar structure, but with the distance halved, so that the dimensions are those of the right-hand side insert in the figure. Due to the reduced length, the interference peaks are now less pronounced. In computing both curves, N was assumed equal to 6; four modes were considered accessible in the larger guide, and two in the standard guide.

Curve 3 in the figure refers to configuration 2. This curve was computed by averaging the small obstacle and the aperture results of [4]. Owing to the large difference in guide widths, the equivalent network given in [4] becomes inaccurate even below 10 GHz.

CONCLUSIONS

Starting from the Rayleigh–Ritz stationary solution of the inductive iris and step in rectangular waveguide, a true lumped equivalent network model has been derived for this type of discontinuity. The features of the method are as follows.

1) The reactance matrix shows good convergence properties, monotonically depending upon only one parameter N, and "relative convergence" effects do not arise. Also, manipulations with only small and well-conditioned matrices are involved.

2) The elements of the equivalent circuit, given in the canonical Foster's form, depend solely upon geometry. Herewith, the frequency characteristics of the discontinuity are described over a wide band. The band can be prescribed and, together with the geometrical configuration, determines the number of accessible ports in the equivalent network.

3) The field analysis of a cascade of interacting discontinuities is transformed into the standard network problem of analyzing a cascade of multiports (generally with a small number of ports), separated by transmission lines. This does away with the need of repeating the field analysis at each "spot frequency." Also, it opens the way to exact network synthesis, with prescribed frequency characteristics, of subsystems and components consisting of cascades of step discontinuities.

APPENDIX I

The reactive part of the magnetic Green's function for the problem depicted in Fig. 2 is

$$-jB_1(x,\xi) = \sum_{n>k} \frac{y_n}{y_1}\left(\frac{2}{a}\right)^{1/2} \sin\frac{n\pi}{a}x \cdot \left(\frac{2}{a}\right)^{1/2} \sin\frac{n\pi}{a}\xi + \sum_{m>k'} \frac{y_m'}{y_1}\left(\frac{2}{a'}\right)^{1/2} \sin\frac{m\pi}{a'}x' \cdot \left(\frac{2}{a'}\right)^{1/2} \sin\frac{n\pi}{a'}\xi' \tag{I1}$$

where

$$\frac{y_n}{y_1} = -j\frac{\Gamma_n}{\beta} \qquad \frac{y_m'}{y_1} = -j\frac{\Gamma_m'}{\beta}.$$

The preceding series is not convergent in the classical sense, but is in fact a generalized function. Numerically, the problem is avoided by double partial integration with a trial field and taking account of the boundary conditions ($E_t = 0$) at the iris edges, as discussed by Collin [8,p.349].

It can be shown that a variational expression for the reactance matrix X of the discontinuity is

$$X_{ij} = \frac{\left(\int g_i E\,dx\right)\left(\int g_i F\,dx\right)}{\iint E \cdot B_1 \cdot F\,dx\,d\xi}, \qquad 1 \le i,\ j \le k_a \tag{I2}$$

where

$$g_i = \left(\frac{2}{a}\right)^{1/2} \sin\frac{i\pi}{a}x, \qquad i \le k$$

$$g_i = \left(\frac{2}{a'}\right)^{1/2} \sin \frac{i\pi}{a'} x', \qquad k+1 \leq i \leq k_a$$

and E,F are "trial fields."

By carrying out double partial integration and upon application of the boundary conditions at the iris edge, we obtain

$$X_{ij} = \tau_i \tau_j \frac{\left[\int (dE/dx) h_i \, dx\right]\left[\int (dF/dx) h_j \, dx\right]}{\iint (dE/dx) \boldsymbol{B} (dF/d\xi) \, dx \, d\xi} \tag{I3}$$

where

$$h_i = \begin{cases} \cos (i\pi/a) x = \phi_i, & i \leq k \\ \cos (i\pi/a') x' = \psi_i, & k+1 \leq i \leq k_a. \end{cases}$$

The quantities φ, ψ, and $\boldsymbol{B}$ are those defined in (1); τ_i is defined in connection with (9). Using the matrix representation introduced in (2)–(7) it can be shown [6] that (I3) can be written as

$$X_{ij} = \tau_i \tau_j Q_{*i}^T \cdot B^{-1} \cdot Q_{*j}$$

which is formula (9) of Section II.

APPENDIX II

Here we shall derive a recursive formula for the coefficients P_{np} of (3).

Consider the recursive formula for the Chebyshev polynomials of the first kind:

$$T_n(x) = 2xT_{n-1}(x) - T_{n-2}(x) \tag{II1}$$

and set in the above

$$\cos \frac{n\pi}{a} x = T_n\left(\cos \frac{\pi}{a} x\right) = T_n(\alpha_1 + \alpha_2 \cos \vartheta). \tag{II2}$$

Using the trigonometric identity,

$$\cos \vartheta \cdot \cos p\vartheta = \frac{1}{2}[\cos (p-1)\vartheta + \cos (p+1)\vartheta]$$

(II1) becomes

$$\sum_{p=0}^{n} P_{np} \cos p\vartheta = 2\alpha_1 \sum_{p=0}^{n-1} P_{n-1,p} \cos p\vartheta - \sum_{p=0}^{n-2} P_{n-2,p} \cos p\vartheta + \alpha_2 \sum_{p=-1}^{n-2} P_{n-1,p+1} \cos p\vartheta + \alpha_2 \sum_{p=1}^{n} P_{n-1,p-1} \cos p\vartheta. \tag{II3}$$

Considering coefficients of $\cos p\vartheta$, yields

$$P_{np} = 2\alpha_1 P_{n-1,p} - P_{n-2,p} + \alpha_2 P_{n-1,p+1} + \alpha_2 \delta_{1,p} P_{n-1,0} + \alpha_2 P_{n-1,p-1} \tag{II4}$$

where

$$\delta_{1,p} = \begin{cases} 0, & p \neq 1 \\ 1, & p = 1 \end{cases}$$

$$P_{00} = 1, \quad P_{10} = \alpha_1, \quad P_{11} = \alpha_2$$

and

$$P_{np} = 0, \qquad \text{if } n < p \text{ or } p < 0.$$

(II4) is the sought recursive formula.

REFERENCES

[1] R. F. Harrington, *Field Computation by the Moment Method*. New York: Macmillan, 1964.

[2] J. Schwinger and D. Saxon, *Discontinuities in Waveguides*. New York: Gordon and Breach, 1968.

[3] T. Itoh and R. Mittra, "A method for solving boundary value problems associated with a class of doubly modified Weiner–Hopf structures," *Proc. IEEE* (Lett.), vol. 57, pp. 2170–2171, Dec. 1969.

[4] N. Marcuvitz, *Waveguide Handbook* (M.I.T. Radiation Laboratory Series). New York: McGraw-Hill, 1951.

[5] T. E. Rozzi, "Hilbert space approach for the analysis of multimodal transmission lines and discontinuities," in *1972 NATO Symp. Network and Signal Theory* (Bournemouth, England), J. Scanlan and J. Skwirzynski, Ed. London, England: Peregrinus, 1973.

[6] T. E. Rozzi, "Network analysis of strongly coupled transverse apertures in waveguide," *Int. J. Circuit Theory Appl.*, vol. 1, pp. 161–179, 1972.

[7] T. E. Rozzi and W. F. G. Mecklenbräuker, "Field and network analysis of waveguide discontinuities," in *Proc. 1973 European Microwave Conf.*, vol. 1, Paper B-1-2.

[8] R. Collin, *Field Theory of Guided Waves*. New York: McGraw-Hill, 1960, ch. 8.

[9] T. E. Rozzi, "The variational treatment of thick interacting inductive irises," *IEEE Trans. Microwave Theory Tech.*, vol. MTT-21, pp. 82–88, Feb. 1973.

[10] D. S. Jones, *The Theory of Electromagnetism*. New York: Pergamon, 1964, ch. 4.

[11] V. Belevitch, *Classical Network Theory*. San Francisco, Calif.: Holden-Day, 1968, ch. 8.

[12] H. J. Butterweck, "A theorem about lossless reciprocal three-ports," *IEEE Trans. Circuit Theory* (Corresp.), vol. CT-15, pp. 74–76, Mar. 1968.